ARTICLES
PUBLISHED ONLINE: 7 AUGUST 2011 | DOI: 10.1038/NNANO.2011.112
nature nanotechnology

Ferri-liposomes as an MRI-visible drug-delivery system for targeting tumours and their microenvironment

Georgy Mikhaylov[1], Ursa Mikac[2,3], Anna A. Magaeva[4], Volya I. Itin[4], Evgeniy P. Naiden[4], Ivan Psakhye[1†], Liane Babes[5], Thomas Reinheckel[5,6], Christoph Peters[5,6], Robert Zeiser[7], Matthew Bogyo[8], Vito Turk[1,9], Sergey G. Psakhye[4,10], Boris Turk[1,9,11,12]* and Olga Vasiljeva[1]*

The tumour microenvironment regulates tumour progression and the spread of cancer in the body. Targeting the stromal cells that surround cancer cells could, therefore, improve the effectiveness of existing cancer treatments. Here, we show that magnetic nanoparticle clusters encapsulated inside a liposome can, under the influence of an external magnet, target both the tumour and its microenvironment. We use the outstanding T_2 contrast properties (r_2 = 573–1,286 s^{-1} mM^{-1}) of these ferri-liposomes, which are ~95 nm in diameter, to non-invasively monitor drug delivery *in vivo*. We also visualize the targeting of the tumour microenvironment by the drug-loaded ferri-liposomes and the uptake of a model probe by cells. Furthermore, we used the ferri-liposomes to deliver a cathepsin protease inhibitor to a mammary tumour and its microenvironment in a mouse, which substantially reduced the size of the tumour compared with systemic delivery of the same drug.

Cancer is the second leading cause of death after cardiovascular diseases in developed countries. Despite rapid developments in medicinal and pharmaceutical chemistry, chemotherapy is still a major challenge. In the last decade, the development of effective targeted drug delivery systems for treating cancer has been a top priority in biomedical technology. However, although there have been methodological advances, stromal tumour components (termed the tumour microenvironment[1]) are generally not included in the treatment area. Recently, the tumour-cell-centred view of the metastatic process has been revised, and research regarding crosstalk between tumour cells and their surrounding tissue supports the notion that the microenvironment determines tumour progression at least as much as the tumour cells[2]. Thus, targeting the stromal cells that constitute an integral part of the cancer is a strategy that could greatly increase the effectiveness of traditional anticancer treatments. The tumour microenvironment includes many diverse components, including extracellular matrix components and various stroma cells, so active targeting mediated by a specific ligand is not possible. An effective delivery system that will target both tumours and their stromal components remains to be developed[3].

Magnetic drug targeting, using magnetic nanoparticles and an external magnetic field focused on the target tissue, has already been described as a promising approach for the specific delivery of therapeutic agents[4–9]. Moreover, magnetic nanoparticles have recently gained additional attention because of their potential as contrast agents for noninvasive magnetic resonance (MR) imaging (MRI)[10–15]. Two types of MR contrast agents are used to enhance the visualization of properties correlated with patient anatomy and physiology: T_1 contrast agents that shorten the spin–lattice relaxation time of nearby protons, and T_2 contrast agents that enhance spin–spin relaxation to reduce the signal of media-containing structures. Currently, the most prominent T_2 contrast agents are based on super-paramagnetic iron oxide nanoparticles, which, in contrast to the T_1 contrast agents, remain intravascular for a longer time, enabling a longer image-acquisition time window.

We have developed a universal lipidated magnetic nanocarrier (called a ferri-liposome) that has enhanced MRI contrast properties and is effectively taken up by tumours and their stromal components. Chemical compounds within the ferri-liposomes are successfully released when administered *in vivo* and can be visualized at tissue and cellular levels.

Development and characterization of ferri-liposomes

Ferrimagnetic iron oxide (magnetite, Fe_3O_4; FMIO) nanoparticles were prepared by mechanochemical synthesis using saline crystal hydrates[16]. The use of saline crystal hydrates instead of conventional methods using anhydrous salts changes the solid-phase mechanism to a soft mechanochemical synthesis in aqueous media, resulting in a significantly increased reaction rate. This modification also results in ultrasmall spherical particles with diameters of 3–14 nm (>70% of particles were less than 8 nm; Fig. 1a,b).

[1]Department of Biochemistry and Molecular and Structural Biology, Jozef Stefan Institute, SI-1000 Ljubljana, Slovenia, [2]Department of Condensed Matter Physics, Jozef Stefan Institute, SI-1000 Ljubljana, Slovenia, [3]Centre of Excellence EN-FIST, SI-1000 Ljubljana, Slovenia, [4]Tomsk Scientific Center, Siberian Branch of Russian Academy of Sciences, Tomsk 634055, Russia, [5]Institut für Molekulare Medizin und Zellforschung, Albert-Ludwigs-Universität Freiburg, Freiburg 79104, Germany, [6]BIOSS Centre for Biological Signalling Studies, Albert-Ludwigs-Universität Freiburg, Freiburg 79104, Germany, [7]Department of Hematology and Oncology, University Medical Center Freiburg, Freiburg 79106, Germany, [8]Department of Pathology, Microbiology and Immunology, Stanford University School of Medicine, California 94305, USA, [9]Center of Excellence CIPKEBIP, SI-1000 Ljubljana, Slovenia, [10]Institute of Strength Physics and Materials Science, Tomsk 634021, Russia, [11]Faculty of Chemistry and Chemical Technology, University of Ljubljana, SI-1000 Ljubljana, Slovenia, [12]Center of Excellence Nanosciences and Nanotechnology, SI-1000 Ljubljana, Slovenia; †Present address: Department of Molecular Cell Biology, Max Planck Institute of Biochemistry, Martinsried 82152, Germany. *e-mail: olga.vasiljeva@ijs.si; boris.turk@ijs.si

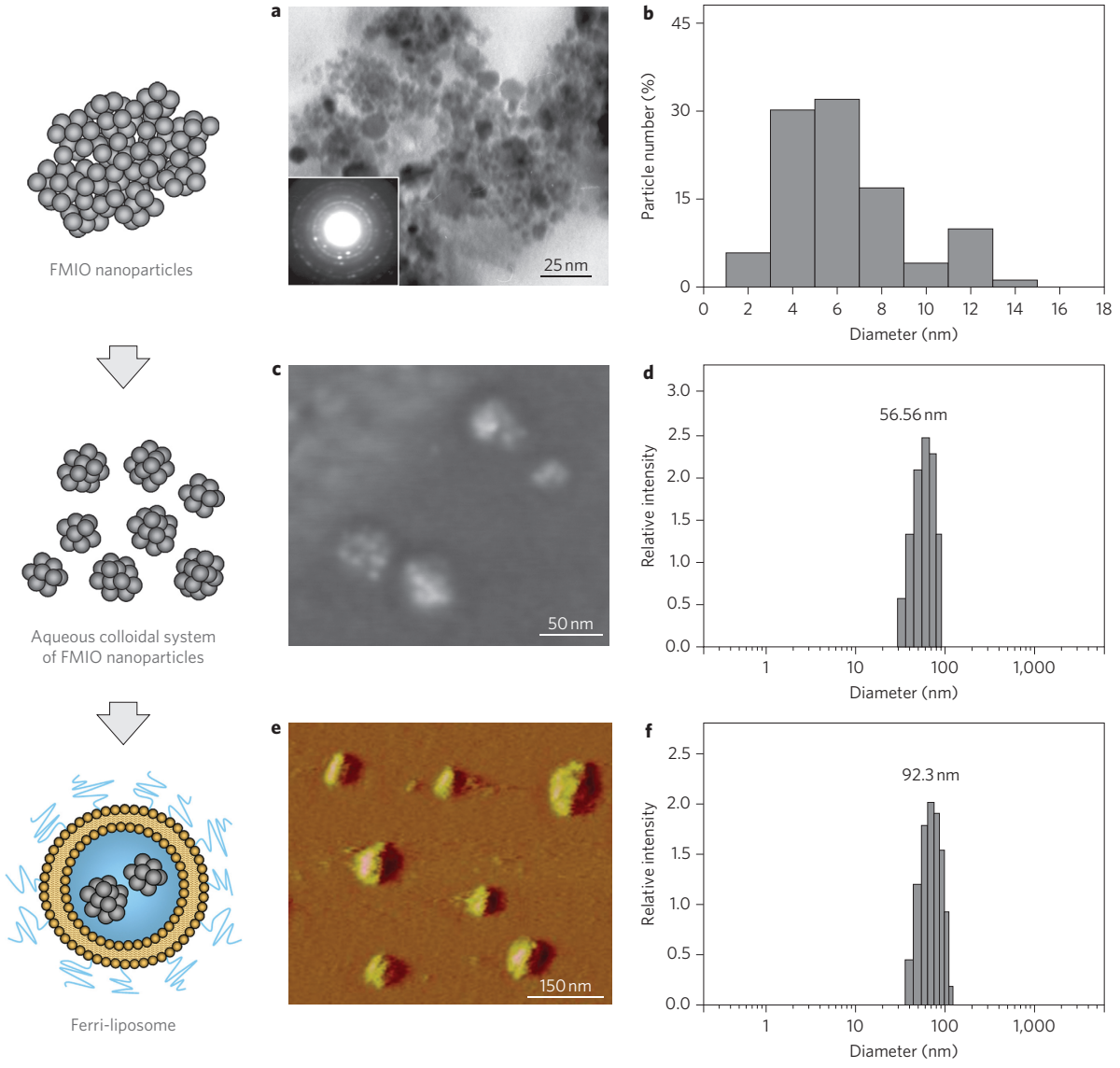

Figure 1 | Characterization of the magnetic nanocarrier system. Schematic on the left corresponds to the experimental data on the right. **a**, Transmission electron micrographs of FMIO nanoparticles. Inset: corresponding electron diffraction pattern. **b**, Size distribution of FMIO nanoparticles (average size, $D = 6.65$ nm). **c**, Field-emission gun scanning electron microscopy of the aqueous colloidal system of FMIO nanoparticles. **d**, DLS measurement of FMIO colloidal dispersion showing the distribution of diameters of the nanoparticle clusters and their average size ($D = 56.56$ nm). **e**, AFM image of liposome-encapsulated FMIO nanoparticles (ferri-liposome). **f**, Liposome size as determined by DLS (average size, $D = 92.3$ nm).

The main limiting factor in using magnetic nanoparticles *in vivo* is their low colloidal stability. Therefore, to prevent their agglomeration, we developed an optimized two-step procedure for preparing a biocompatible aqueous colloidal system from powdered FMIO nanoparticles, leading to a narrower particle size distribution of nanoclusters (Fig. 1c; see Supplementary Methods). The concentration of FMIO nanoparticles was measured by flame atomic absorption spectrometry, and the unit average size of nanoparticles was determined by dynamic light scattering (DLS) (Fig. 1d). The resulting FMIO nanoparticles had a negative surface zeta potential of 27.9 ± 4.3 mV at pH 7.4 and 37 °C. In addition, their suspension exhibited high colloidal stability under physiological conditions as well as at other pH values and ionic strengths (Supplementary Fig. S1).

Magnetic nanoparticles encapsulated within a phospholipid bilayer, forming liposomes, have been reported to have considerable structural and pharmacokinetic advantages for drug delivery[11,17,18]. Owing to their ability to encapsulate both hydrophobic and hydrophilic therapeutics, they prevent local dilution of the drug and limit its interaction with the surrounding environment, enabling reduction of the therapeutic dose and toxicity. In the present work, stabilized FMIO nanoparticles were encapsulated in sterically stabilized polyethylene glycol (PEG)-coated liposomes (PEGylated, Stealth Liposomes), forming ferri-liposomes with a diameter of 100 nm. Modification of the liposome surface with PEG is known to greatly reduce the opsonization of liposomes and their subsequent clearance by the reticuloendothelial (mononuclear-phagocyte) system[11,19–21], resulting in a substantially prolonged circulation half-life. This was confirmed in a cellular experiment (Supplementary Fig. S2). The liposomes loaded with FMIO particles appeared, under atomic force microscopy (AFM), as spheroids with diameters of 0.09–0.11 μm (Fig. 1e), consistent with the average diameter of 92.3 nm measured for ferri-liposomes using DLS (Fig. 1f). Because of their size, hydrophobic and hydrophilic character and biocompatibility, together with their internal hollow space (Supplementary Fig. S3), the system of ferri-liposomes

enables simultaneous encapsulation of FMIO nanoparticles with other substances such as pharmaceutical drugs or DNA, and their subsequent targeted delivery in an organism.

MR contrast properties of FMIO nanoparticles

The MR contrast properties of the stabilized FMIO nanoparticles were evaluated *in vitro* using 1% agarose phantoms ($T_2 \approx 80$ ms), which simulate tumour tissue[22]. The phantoms contained two types of FMIO nanoparticles with mean hydrodynamic diameters of 39 nm and 57 nm, respectively. The longitudinal (T_1) and transverse (T_2) relaxation times were measured at different concentrations of FMIO nanoparticles, and the relaxivities were determined to be $r_1 = 12\ s^{-1}\ mM^{-1}$ and $r_2 = 573\ s^{-1}\ mM^{-1}$ for the 39 nm nanoparticles and $r_1 = 31\ s^{-1}\ mM^{-1}$ and $r_2 = 1{,}286\ s^{-1}\ mM^{-1}$ for the 57 nm nanoparticles (Fig. 2a). FMIO nanoparticles showed several-fold higher relaxivities than commercially available super-paramagnetic iron oxide nanoparticles (Feridex, Bayer HealthCare Pharmaceuticals)[23] and the standard gadolinium-based T_1 contrast agent Magnevist (Bayer HealthCare Pharmaceuticals) (Fig. 2a). Moreover, a 20–70% improvement in the r_2 relaxivity was found when compared to the best iron oxide-based nanoparticles described in the literature[24–26]. The high r_2 relaxivity may be due to clustering of the FMIO nanoparticles[24,27,28], and this is further supported by the higher relaxivity observed for nanoparticles with a higher hydrodynamic diameter of clusters. These results show that FMIO nanoparticles are high-performance MRI contrast agents that enable highly sensitive T_2-weighted MRI measurements.

To verify the effectiveness of the FMIO nanoparticles as positive T_1 and negative T_2 contrast agents, we obtained T_1-weighted and T_2-weighted images of the control phantom and of phantoms with 0.017 mM and 0.17 mM each of the 39 nm and 57 nm FMIO nanoparticles (Fig. 2b). The signal intensity of these phantoms was significantly diminished on the T_2-weighted MR scans, whereas the same concentration of FMIO nanoparticles demonstrated enhanced MRI signal on the T_1-weighted images compared to the control phantom (Fig. 2b). Hence, unique simultaneous T_1 and T_2 MR contrast properties of FMIO nanoparticles were demonstrated, enabling their use as single contrast agents for both T_1- and T_2-weighted MR scans, thereby enhancing the diagnostic properties of MR imaging. Moreover, the twofold higher sensitivity of the 57 nm FMIO nanoparticles relative to the smaller 39 nm nanoclusters in T_2-weighted MR scans (Fig. 2b) suggests the former to be extremely effective contrast agents. However, in drug-delivery applications the smaller 39 nm nanoclusters, with their still superior contrast properties, are preferable.

To demonstrate the effectiveness of the suspension of magnetic nanoparticles on targeting and their MRI contrast properties, two techniques for delivering FMIO nanoparticles into the agarose phantoms were used: (i) direct injection of the FMIO nanoparticle solution with an 0.3 mm needle into the centre of the phantom (sample 2 in Fig. 2c) and (ii) application of the FMIO nanoparticle dispersion to the phantom surface by positioning the magnetic field ($B = 0.33$ T) at the bottom of the vial (sample 4 in Fig. 2c). The MRI signal intensity was compared with pure agarose phantoms (samples 1 and 3 in Fig. 2c) and normalized to a small probe containing a solution of $CuSO_4{\cdot}H_2O$ (sample 5 in Fig. 2c). As seen on the T_2-weighted MR image and from the MR signal intensity profile (Fig. 2c), both delivery methods were effective, demonstrating a clear difference between the MR signal of the FMIO nanoparticles and the agarose phantom. Moreover, the MR signal of sample 4 disappeared completely, indicating successful penetration of the FMIO nanoparticles through the phantom matter as a result of targeting by an external magnetic field. Collectively, these results demonstrate that FMIO nanoparticles can be used for multifunctional targeted delivery, enabling simultaneous MR detection. In addition, the MRI contrast properties of FMIO nanoparticles remain the same after their encapsulation into the liposomes (Supplementary Fig. S4), supporting the use of ferri-liposomes in medical applications.

Ferri-liposome as MRI-visible drug delivery system *in vivo*

To establish the efficacy of the prepared ferri-liposomes for *in vivo* applications we used a genetically engineered mouse model of human breast cancer (MMTV-PyMT), resulting in a widespread transformation of the mammary epithelium and the development of multifocal mammary adenocarcinomas[29]. Ferri-liposomes were first demonstrated to be non-cytotoxic in mouse embryonic fibroblasts (MEFs) and primary mouse tumour cells (Supplementary Fig. S5). Possible adverse effects of FMIO nanoparticles were also evaluated in an acute toxicity experiment using rats. No significant differences in blood biochemistry or histopathological analysis were observed 7 and 12 days after administration between control animals and animals treated with 500 mg kg^{-1} FMIO nanoparticles (Supplementary Table S1 and Fig. S6). Having shown that the system was suitable for *in vivo* applications, ferri-liposomes were injected intraperitoneally into an MMTV-PyMT tumour-bearing mouse while a magnetic field was applied for 1 h to the first left inguinal mammary tumour. Tumour tissue with a high MR signal appears yellow-red on T_2-weighted MR images (Fig. 3a), while FMIO nanoparticles delivered by ferri-liposomes appear as a dark area, 1 and 48 h post-injection (Fig. 3a, Supplementary Fig. S7), confirming their successful targeting to the tumour region and their apparent MRI contrast effect. Furthermore, as well as spreading through the tumour tissue, nanoparticles were detected in the tumour surroundings, the tumour microenvironment (Supplementary Fig. S7). This ability of ferri-liposomes could be of particular value for developing novel strategies to treat cancer, with the further advantage of the possibility of being regulated by a magnetic field (Supplementary Fig. S8). The effectiveness of the system was confirmed by intravenous administration of ferri-liposomes (Supplementary Fig. S9). Collectively, these results demonstrate both the efficacy of ferri-liposomes for magnetic field targeted drug delivery and the possibility of monitoring their distribution by non-invasive MRI technology.

The intracellular delivery of targeted ferri-liposomes was validated in tumour and stromal cells using a fluorescent marker (Alexa Fluor 555) as a model drug. The Alexa Fluor 555- functionalized ferri-liposome suspension was incubated for 3 h with primary MMTV-PyMT tumour cells and MEFs. Fluorescence microscopy analysis revealed very efficient internalization of the Alexa Fluor 555 by both types of cells (Fig. 3b). Moreover, compartmentalization of fluorescent particles in intracellular vesicles of primary tumour cells and fibroblasts provides clear evidence for successful endocytosis of the ferri-liposome cargo. This carrier system therefore represents a promising candidate for targeted drug delivery into both the tumour and its microenvironment, enabling more effective cancer therapy.

To confirm the release of drug encapsulated in ferri-liposomes *in vivo*, we crossed MMTV-PyMT mice ($PyMT^{tg/+}$) with the FVB/N mouse strain expressing firefly luciferase under the control of the ß-actin promoter ($FVB.luc^{tg/+}$)[30]. The resulting double transgenic mice ($FVB.luc^{tg/+};PyMT^{tg/+}$) develop breast tumours with simultaneous expression of luciferase throughout the body. Twenty four hours after administration and targeting of ferri-liposomes loaded with the luciferase substrate (D-luciferin) to the tumour, a luminescent signal was imaged exclusively in the tumour region exposed to the 0.33 T magnet (Fig. 3c), indicating effective release of the cargo from the targeted ferri-liposomes *in vivo*. The efficiency of the system was also confirmed by intravenous administration of ferri-liposomes (Supplementary Fig. S10). Furthermore, nanoparticles were successfully excreted from the body without any evident accumulation (Supplementary Fig. S11, S12), which fulfils another critical parameter for their *in vivo* application.

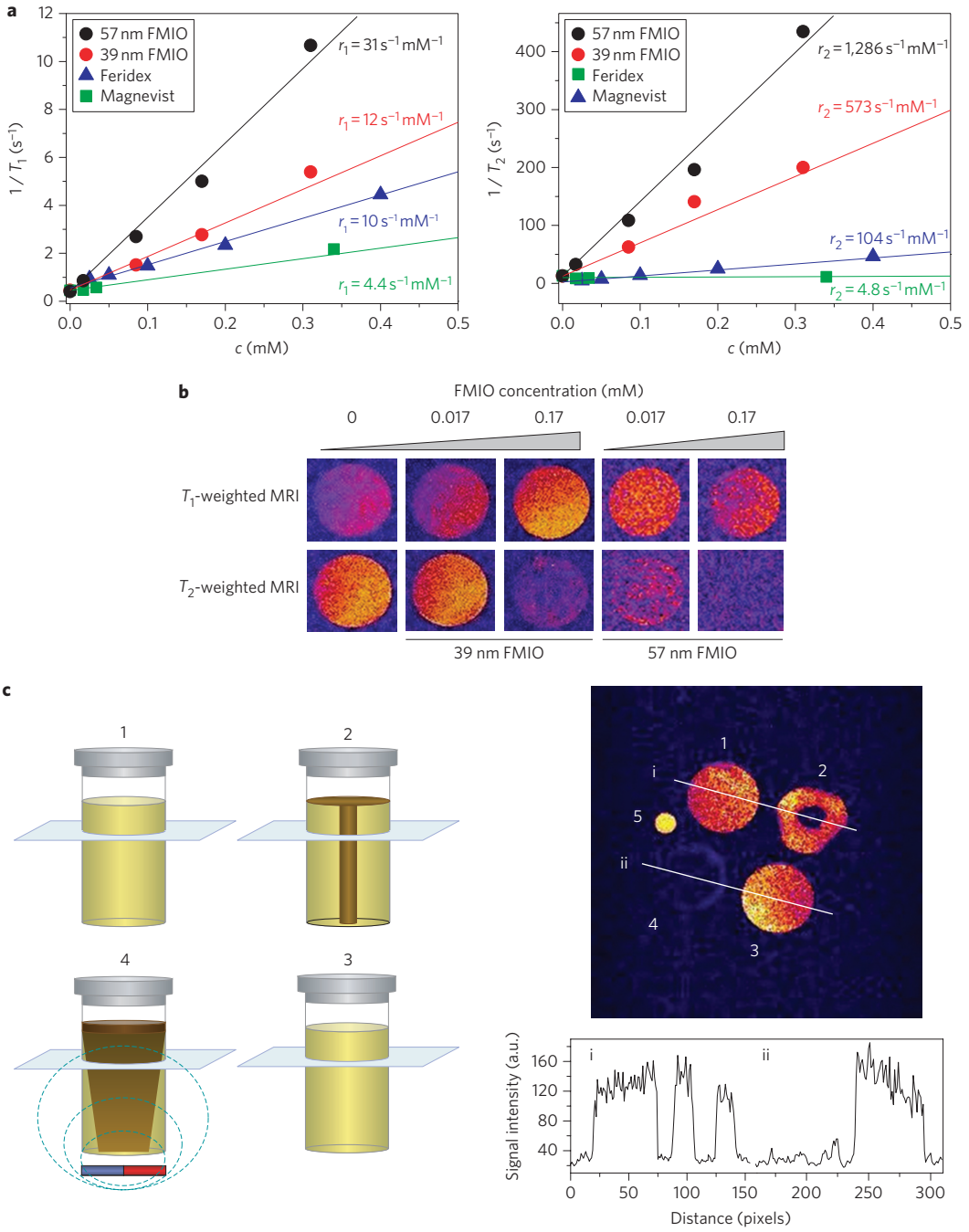

Figure 2 | MR contrast properties of electrostatically stabilized FMIO nanoparticles. a, Spin–lattice $1/T_1$ (left) and spin–spin $1/T_2$ (right) relaxation rates of 39 nm and 57 nm FMIO nanoparticles at different concentrations, compared to commercially available MR contrast agents (Ferridex[17] and Magnevist). Relaxivity rates r_1 and r_2 were obtained by comparing the measured (symbols) and theoretical (lines) values. **b**, T_1- and T_2-weighted MR images of agarose phantoms at different concentrations of 39 nm and 57 nm FMIO nanoparticles. **c**, Schematic (left) and T_2-weighted MR image (right) of four phantom-probes containing 1% agarose (samples 1 and 3), and 3.4 mM FMIO nanoparticles either injected into the centre of the 1% agarose gel (sample 2) or diffused into the 1% agarose in the presence of a magnetic field (sample 4). Bottom panel shows signal intensity profiles along lines i and ii. Sample 5 is a small probe containing a solution of $CuSO_4{\cdot}H_2O$ in the phantom.

Ferri-liposome delivers cargo to inhibit tumour growth

Initial testing of the ferri-liposome system for targeted drug delivery was performed with a standard cancer chemotherapy drug, doxorubicin. Even a single-dose treatment with doxorubicin targeted by ferri-liposomes resulted in a 90% reduction of tumour volume two weeks after administration, compared with a 60% decrease obtained by standard doxorubicin administration (Supplementary Fig. S13). However, we aimed at a bigger challenge: to convert a compound known to be ineffective due to poor bioavailability into an effective one. For this purpose we selected JPM-565, a small-molecule broad-spectrum inhibitor of cysteine cathepsins[31,32], which is very potent in treating pancreatic islet cell cancer in a mouse model[33,34]. However, due to its very poor bioavailability, JPM-565 is not effective in the MMTV-PyMT mouse breast cancer model[35], but, through genetic ablation of several cathepsins, tumour progression in this breast cancer model can be attenuated[36–38]. There is increasing evidence that cysteine cathepsins contribute to tumour progression via several possible mechanisms, including

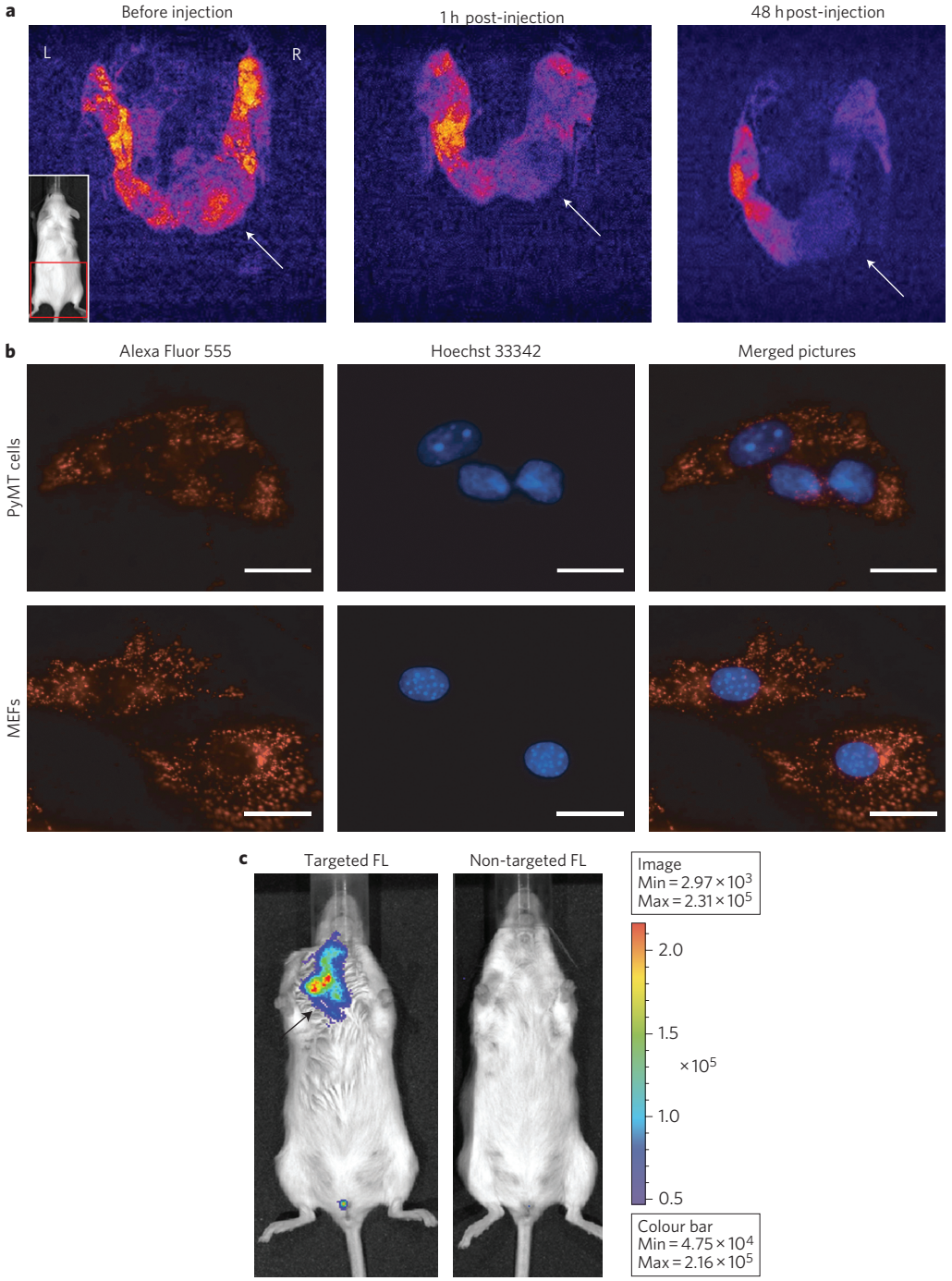

Figure 3 | Monitoring the targeting and release of ferri-liposomes *in vivo*. **a**, T_2-weighted MR images of an MMTV-PyMT transgenic mouse before and 1 h and 48 h after intraperitoneal injection of ferri-liposomes followed by 1 h of magnetic field application to the lower right tumour (white arrow). Inset: red rectangle shows the region of the MRI images. **b**, Fluorescence images of primary MMTV-PyMT tumour cells and MEFs incubated with Alexa Fluor 555-functionalized ferri-liposomes for 3 h at 37 °C. Scale bar, 20 μM. Data are representative of three separate experiments. **c**, Optical imaging of FVB.luc$^{tg/+}$;PyMT$^{tg/+}$ mice that have been intraperitoneally administered with ferri-liposomes (FL) carrying D-luciferin in the presence (targeted FL) and absence (non-targeted FL) of magnet application. A high-intensity luciferase signal was detected only in the tumour region exposed to the magnet (black arrow). The scale is in photons s^{-1} sm^{-2} sr^{-1}.

activation of the extracellular proteolytic cascade(s), degradation of the extracellular matrix, and inactivation of adhesion molecules such as E-cadherin[37,39]. Their inhibition could therefore form a potent strategy for tumour treatment[40]. Moreover, the cysteine cathepsins participating in multiple stages of tumour progression[37,38,41–43] originate largely from the cells of the microenvironment[36,44,45], thereby offering the opportunity to simultaneously validate the novel concept of targeting the tumour microenvironment as well as the novel drug delivery system in order to improve cancer treatment.

To overcome the limitations of the transgenic MMTV-PyMT mouse model having multifocal mammary tumours that are difficult to follow, and to secure the functional immune system (as compared to the xenograft approach), an orthotopically transplanted mouse mammary tumour model was developed by inoculating 5×10^5

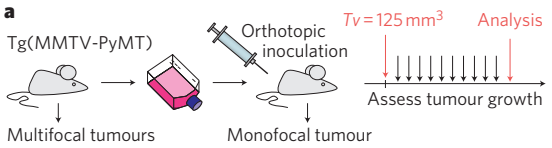

b

Groups	JPM-565	Ferri-liposome	Magnet
Control	–	–	–
FLt		+	+
JPM	+	–	–
JPM + FL		+	
JPM + FLt			+

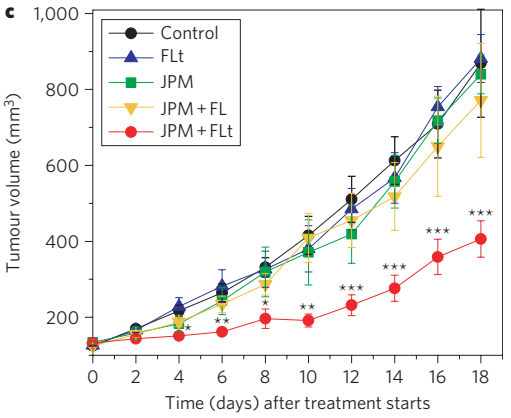

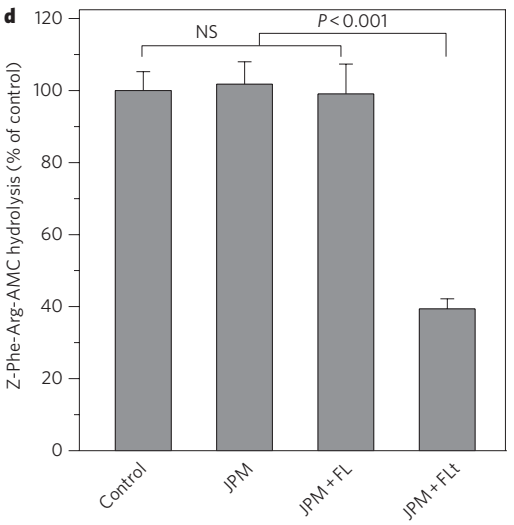

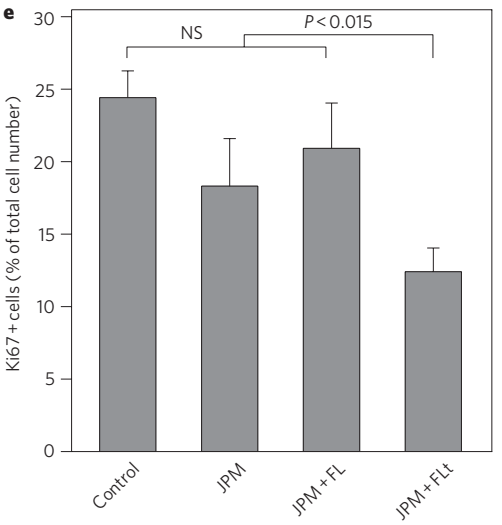

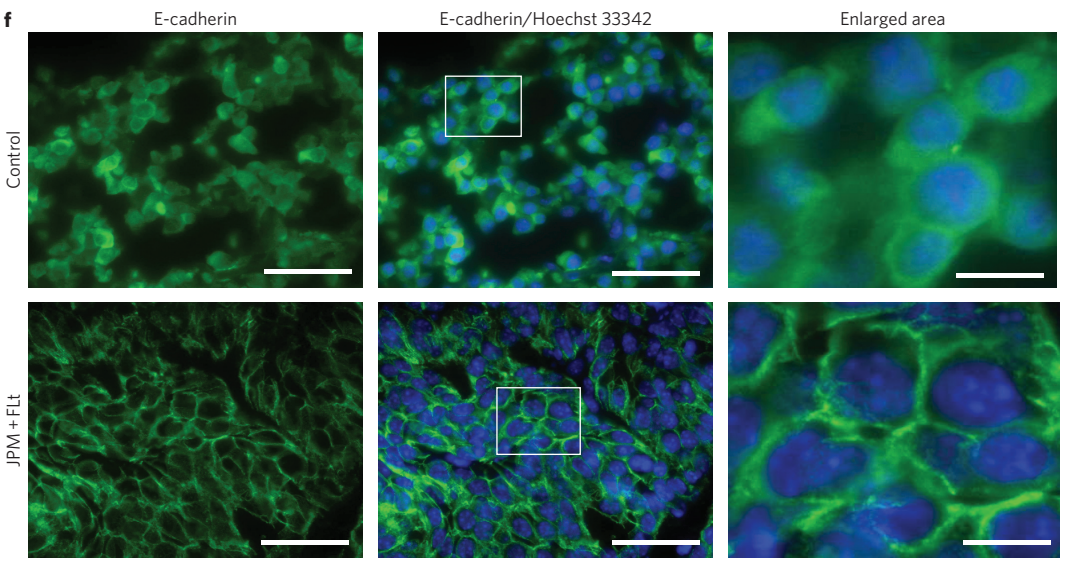

Figure 4 | Anti-tumour effect of magnetically targeted ferri-liposomes containing cysteine protease inhibitor JPM-565. a, Schematic showing the treatment experiment design. Cells from the transgenic (Tg) MMTV-PyMT mouse with multifocal tumours were cultured and inoculated into an immunocompetent FVB/N mouse to form a model with a monofocal tumour that can be easily monitored. **b**, Table showing the treatment groups. Mice were treated with stabilizing buffer containing different compounds and magnetic targeting combinations as represented by the '+' and '−' signs. **c**, Tumour volumes for each treatment day for the different treatment groups. $^{*}P < 0.05$, $^{**}P < 0.01$ and $^{**}P < 0.001$, compared with the other groups. **d**, Activity of cysteine cathepsins in tumour tissue after JPM-565 administration (NS, not significant). **e**, The percentage of $Ki67^{+}$ cells as calculated by computer-assisted data analyses. Data are presented as means and standard errors, $n = 5$. Statistics were analysed using Student's *t*-test. NS, not significant. **f**, Fluorescent images of control tumours and tumours treated with JPM-565 targeted by ferri-liposomes (JPM + FLt). E-cadherin is stained green and nucleus is stained with Hoechst 33342 (blue). Higher-magnification images (right column) of white rectangles from the middle column illustrate the different patterns of E-cadherin localization. Scale bars, 100 μm and 25 μm (higher magnification images).

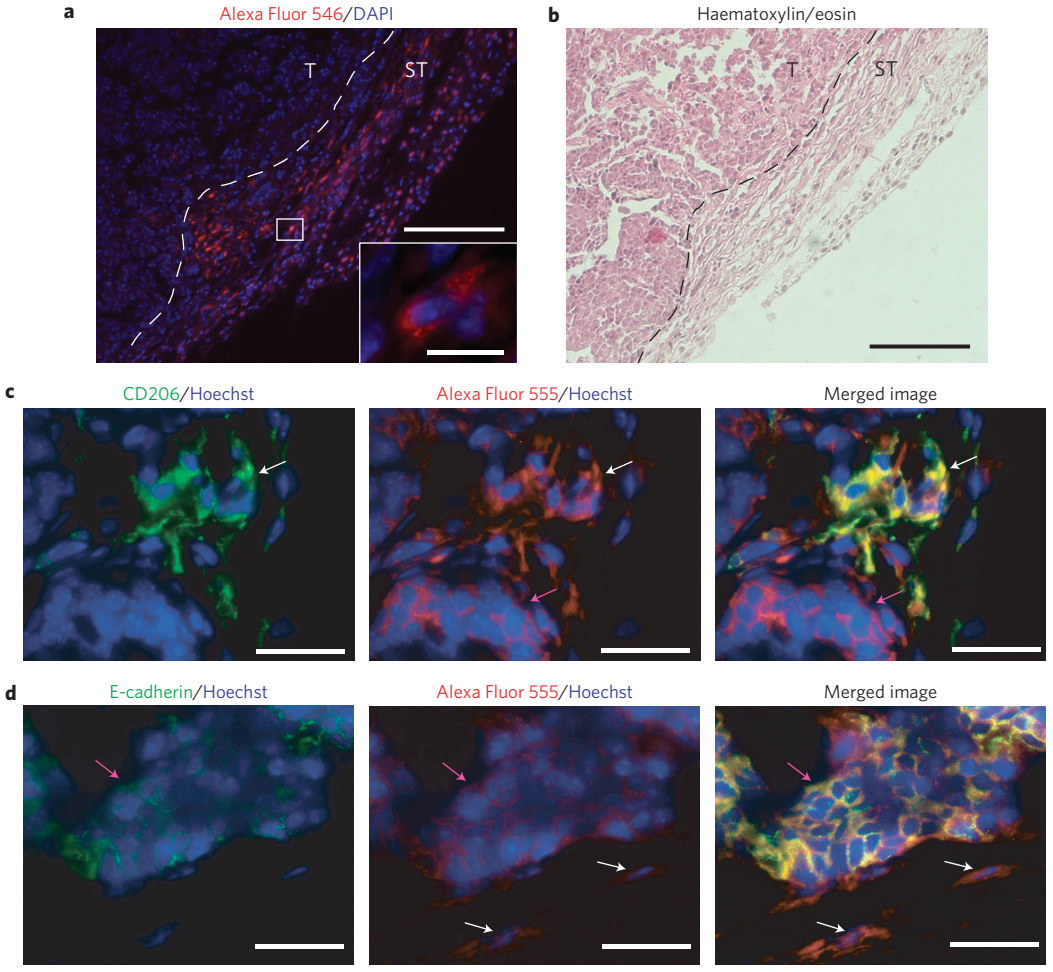

Figure 5 | *In vivo* detection of fluorescent ferri-liposomes in tumours. a, Fluorescent images of tissues confirm the presence of intraperitoneally administered Alexa Fluor 546-functionalized ferri-liposomes (red) in the tumour microenvironment. Inset: higher-magnification image of an individual cell of the tumour stroma outlined by the white rectangle in the main panel. **b**, Haematoxylin and eosin staining of the corresponding section. Stromal (ST) and tumour (T) compartments of the tumour tissue are indicated, with their boundary demarcated by a dotted line. Scale bars in **a** and **b**, 200 μm and 20 μm (inset). **c**,**d**, Uptake of Alexa Fluor 555-functionalized ferri-liposomes (red) by both stroma (white arrows) and tumour cells (pink arrows), after double intravenous injection of ferri-liposomes. Tissues were co-stained with tumour-associated macrophages (CD206-FITC; green) in **c** and tumour cell marker (E-cadherin; green fluorescence) in **d**. Scale bars in **c** and **d**, 40 μm.

primary MMTV-PyMT tumour cells into the mammary gland of a congenic immunocompetent recipient mouse (FVB/N mouse strain) (Fig. 4a). In contrast to the original transgenic model, the orthotopic transplanted model results in a single tumour that can be easily monitored due to the lower heterogeneity regarding tumour latency and growth, thus making it an ideal model for drug efficacy studies.

Starting with a tumour volume of 125 mm^3, ferri-liposomes containing JPM-565 at a concentration of 100 mg kg^{-1} were injected intraperitoneally 10 times every second day with a magnetic field focused on the tumour (Fig. 4a). Tumour sizes were measured the day after each injection. At the end of treatment, tumours were excised and their volumes determined. The anti-tumour effect of non-loaded ferri-liposomes and different therapeutic modalities and forms of JPM-565 were compared (Fig. 4b). Mice treated with targeted JPM-565 loaded ferri-liposomes displayed a significant lag in tumour growth (as exemplified by the smaller tumours; Supplementary Fig S14) compared with all other groups (Fig. 4c), suggesting cathepsin inhibition was successful. This was confirmed by the substantial reduction of cysteine cathepsin activity measured exclusively in tumour samples from this group (Fig. 4d), which contrasts with the observation of no difference in cathepsin expression in all the groups (Supplementary Fig. S15). In agreement with previous studies[33,35], a significant inhibition of cysteine cathepsins was observed in organs close to the peritoneum (Supplementary Fig. S16). Subsequent clearance from the peritoneum through the lymph nodes was also confirmed (Supplementary Fig. S17).

To address the role of cysteine cathepsins in tumour biological processes, we investigated the effect of cathepsin inhibition on tumour proliferation, vascularization and invasiveness. Cell proliferation was quantified by immunohistochemical detection of the proliferation marker Ki67, revealing a significant decrease in the proliferation rate of tumours treated with targeted JPM-565 compared to the other groups (Fig. 4e, Supplementary Fig. 18), corroborating reduced tumour growth in that cohort of mice. Based on the distribution of the endothelial cell marker CD31, no difference in vascularization of the tumour samples was observed following treatment (Supplementary Fig. 19). However, there was a trend for translocation of the cell-adhesion protein E-cadherin from the cytosol to the cell surface following treatment with targeted JPM-565 (Fig. 4f), resulting in decreased invasiveness and progression of the cancer.

To confirm the targeting of JPM-565 to the tumour, the treatment scheme was mimicked by loading ferri-liposomes with a fluorescent marker (Alexa Fluor 546). Evidently, these ferri-liposomes

were successfully targeted to the tumour site, and uptake of their content by cells of the tumour microenvironment was clearly established (Fig. 5a,b). Moreover, we have demonstrated *in vivo* that the marker was compartmentalized in the intracellular vesicles of the tumour stroma cells (Fig. 5a, inset). The latter is of particular importance because cathepsins from tumour stroma are believed to play an important role in the processes leading to tumour progression.

Although intraperitoneal administration of therapeutic agents is an important adjunct to surgery and systemic chemotherapy of cancer in selected patients[46], we have evaluated the effectiveness of intravenous administration of our delivery system for targeting a tumour and its microenvironment in the MMTV-PyMT transgenic female mouse. The fluorescence of ferri-liposome cargo (Alexa Fluor 555) was found to be co-localized both with the stroma (Fig. 5c, CD206 marker for tumour-associated macrophages) and the tumour cells (Fig. 5d, epithelial marker E-cadherin) in the targeted PyMT tumour tissue. These results clearly demonstrate the potential applicability of the ferri-liposomes in a variety of therapeutic scenarios.

Conclusion

A new delivery platform for targeting both the tumour and its microenvironment, based on ferrimagnetic nanoclusters, has been developed. Ferri-liposomes were shown to act as a universal drug delivery system, confirmed by targeting of several chemically different types of cargo. Furthermore, based on the nanoparticles with superior MRI contrast properties, the ferri-liposome system could provide the non-invasive, real-time MRI strategy with unlimited depth penetration and significantly improved sensitivity. The combination of the favourable biodistribution of these nanoparticles to tumours and their microenvironments, as well as their prominent MRI properties, offers the exciting possibility of the simultaneous delivery and detection of therapeutic agents *in vivo*. The feasibility of this approach was confirmed *in vivo* by the use of the MR technique and fluorescent and bioluminescent markers, revealing ferri-liposomes to be highly promising candidates for cancer treatment. As such, the cathepsin inhibitor JPM-565 was targeted by ferri-liposomes to the peri-tumoral region of mouse breast cancer, resulting in a significant reduction in tumour growth. Overall, we believe that this multifunctional MRI-visible targeted delivery system based on FMIO nanoparticles with superior properties constitutes a major advance in the application of nanotechnologies in medicine, and has opened up new possibilities for the diagnosis and treatment of important human diseases such as cancer.

Methods

Preparation of ferri-liposomes. FMIO nanoparticles (magnetite, Fe_3O_4) were manufactured by mechanochemical synthesis using saline crystal hydrates as described[16]. Sodium chloride, as an inert component, was added in the ratio 1:2. The mixture was sealed by steel balls in a planetary mill, washed with distilled water and, optionally, dried in a laminar flow cabinet at room temperature. FMIO nanoparticles were suspended in a stabilizing buffer (20 mM sodium citrate buffer, pH 7.4, containing 108 mM NaCl, 10 mM HEPES), sonicated (Ultrasonic Disintegrator, Branson) and centrifuged to separate the remaining undisrupted agglomerates. The resulting stable colloidal dispersion of non-aggregating nanoparticle clusters was characterized using flame atomic absorption spectrometry (SpectrAA 110, Varian), DLS (using a PDDLS/BatchPlus System, Precision Detectors) and field-emission gun scanning electron microscopy (SEM) using an FE-SEM SUPRA 35VP (Carl Zeiss). The zeta potential of FMIO nanoparticles was measured by a PALS Zeta Potential Analyzer at pH 7.4 and 37 °C.

FMIO nanoparticle-loaded liposomes (ferri-liposomes) were prepared from 95% L-a-phosphatidylcholine (Avanti Lipids) and 5% 1,2-distearoyl-*sn*-glycero-3-phosphoethanolamine-*N*-[methoxy(polyethylene glycol)-2000] (Avanti Lipids), and purified (Supplementary Methods).

For *ex vivo* and *in vivo* studies, ferri-liposomes were functionalized with Alexa Fluor 546-labelled dextran (Invitrogen), non-conjugated Alexa Fluor 555 (Invitrogen), D-luciferin (Sigma) or JPM-565 (DTP, NCI) (Supplementary Methods).

***In vitro* and *in vivo* MRI.** All MR experiments were performed on a TecMag Apollo MRI spectrometer with a superconducting 2.35 T horizontal bore magnet (Oxford Instruments), using a 25 mm saddle-shaped Bruker RF coil. Spin–lattice and spin–spin relaxation times (T_1 and T_2) were measured for different concentrations of FMIO nanoparticles in 1% agarose at room temperature, using inversion recovery and spin-echo techniques, respectively. The longitudinal (r_1) and transverse (r_2) relaxivities were calculated from $r_i = (1/T_i - 1/T_{i0})/c$, where c is the concentration of FMIO nanoparticles in mM, T_i is the relaxation time at concentration c, T_{i0} is the relaxation time of 1% agarose, and $i = 1$ and 2 for T_1 and T_2, respectively.

Two-dimensional MR images were taken using a standard multislice spin-echo pulse sequence with an echo time (TE) of 8.5 ms and a repetition time (TR) of 400 ms for T_1-weighted MR images, and with $TE = 60$ ms and $TR = 2{,}000$ ms for T_2-weighted MR images. The field of view was 40 mm, with an in-plane resolution of 156 μm and a slice thickness of 1 mm. For *in vivo* detection see Supplementary Fig. S7.

Assessment of ferri-liposome internalization *ex vivo*. Primary MMTV-PyMT cells and mouse embryonic fibroblasts (MEFs) were isolated (Supplementary Methods) and cultured with Alexa Fluor 555-functionalized ferri-liposomes in normal culture medium on Lab-Tek Chamber Slides (Nunc). After incubation for 3 h with nanoparticles, cells were washed with PBS, stained with Hoechst 33342 (Fluka) and examined with an Olympus fluorescence microscope (Olympus IX 81) with Imaging Software for Life Science Microscopy Cell[f].

Assessment of ferri-liposome targeting and internalization *in vivo* by bioluminescence. For *in vivo* control of ferri-liposome distribution and content release, ferri-liposomes functionalized with D-luciferin were administered intraperitoneally (30 mg kg^{-1} of D-luciferin) to a 10-week-old FVB.luc$^{tg/+}$;PyMT$^{tg/+}$ mouse, and a magnet was attached to the first right pectoral mammary tumour. Twenty-four hours after ferri-liposome administration, the magnet was detached and the mouse was imaged non-invasively using an IVIS Imaging System (IVIS 100 Series). In the control experiment the magnet was omitted. During the scan, mice were kept under gaseous anaesthesia (5% isofluorane) and at 37 °C.

Treatment study. Primary MMTV-PyMT tumour cells, obtained as described[36], were culture-expanded, suspended in serum free Dulbecco's Modified Eagle Medium (DMEM) (Invitrogen), and 5×10^5 cells were inoculated into the left inguinal mammary gland of the congenic recipient mouse (FVB/N mouse strain). The dosing regimen for JPM-565 treatment was determined based on previous reports[33–35,47]. JPM-565 had no discernable toxic side effects in the animal trials[33,47]. When tumour volume (Tv) reached 125 mm^3, mice were treated with stabilizing buffer containing either of the compounds (Fig. 4b). JPM-565 was administered at a dose of 100 mg kg^{-1} every second day in 10 intraperitoneal injections, and progression of tumours was investigated (Supplementary Methods). Histological measurement of proliferation by Ki67 staining, and tumour vascularization rate by CD31 staining, were performed as described[38,48].

Analysis of ferri-liposome targeted delivery *in vivo* at the tissue and cellular level. Alexa Fluor 546-functionalized ferri-liposomes were injected intraperitoneally, daily, to the orthotopic transplanted breast cancer mouse model for 3 days. Alexa Fluor 555-functionalized ferri-liposomes were injected intravenously, daily, into the MMTV-PyMT transgenic breast cancer mouse model for 2 days. A magnetic field was applied to the tumour for 12 h immediately after each injection. Rabbit anti-mouse E-cadherin (Abcam) and rat anti-mouse monoclonal FITC-conjugated CD206 (AbD Serotec) were used for Fig. 5c,d (Supplementary Methods).

Statistical analysis. Quantitative data are presented as means ± standard error. Differences were compared using Student's *t*-test. When *P*-values were 0.05 or less, differences were considered statistically significant.

Received 31 January 2011; accepted 16 June 2011; published online 7 August 2011

References

1. Liotta, L. A. & Kohn, E. C. The microenvironment of the tumour-host interface. *Nature* **411,** 375–379 (2001).
2. Mueller, M. M. & Fusenig, N. E. Friends or foes—bipolar effects of the tumour stroma in cancer. *Nature Rev. Cancer* **4,** 839–849 (2004).
3. Santos, A. M., Jung, J., Aziz, N., Kissil, J. L. & Puré, E. Targeting fibroblast activation protein inhibits tumor stromagenesis and growth in mice. *J. Clin. Invest.* **119,** 3613–3625 (2009).
4. Rosi, N. L. & Mirkin, C. A. Nanostructures in biodiagnostics. *Chem. Rev.* **105,** 1547–1562 (2005).
5. Arrueboa, M., Fernández-Pachecoa, R., Ibarraa, M. R. & Santamaría, S. Magnetic nanoparticles for drug delivery. *Nanotoday* **2,** 22–32 (2007).
6. Galanzha, E. I. *et al. In vivo* magnetic enrichment and multiplex photoacoustic detection of circulating tumour cells. *Nature Nanotech.* **4,** 855–860 (2009).
7. Namiki, Y. *et al.* A novel magnetic crystal–lipid nanostructure for magnetically guided *in vivo* gene delivery. *Nature Nanotech.* **4,** 598–606 (2009).

8. Kim, J. W., Galanzha, E. I., Shashkov, E. V., Moon, H. M. & Zharov, V. P. Golden carbon nanotubes as multimodal photoacoustic and photothermal high-contrast molecular agents. *Nature Nanotech.* **4,** 688–694 (2009).
9. Vlaskou, D. *et al.* Magnetic and acoustically active lipospheres for magnetically targeted nucleic acid delivery. *Adv. Funct. Mater.* **20,** 3881–3894 (2010).
10. Bulte, J. W. M. *et al.* Selective Mr imaging of labeled human peripheral-blood mononuclear-cells by liposome mediated incorporation of dextran-magnetite particles. *Magn. Reson. Med.* **29,** 32–37 (1993).
11. Bulte, J. W., de Cuyper, M., Despres, D. & Frank, J. A. Short- vs. long-circulating magnetoliposomes as bone marrow-seeking MR contrast agents. *J. Magn. Reson. Imaging* **9,** 329–335 (1999).
12. Bulte, J. W. M., de Cuyper, M., Despres, D. & Frank, J. A. Preparation, relaxometry, and biokinetics of PEGylated magnetoliposomes as MR contrast agent. *J. Magn. Magn. Mater.* **194,** 204–209 (1999).
13. Lee, J. *et al.* Artificially engineered magnetic nanoparticles for ultra-sensitive molecular imaging. *Nature Med.* **13,** 95–99 (2007).
14. Torchilin, V. Multifunctional and stimuli-sensitive pharmaceutical nanocarriers. *Eur. J. Pharm. Biopharm.* **71,** 431–444 (2009).
15. Medarova, Z., Pham, W., Farrar, C., Petkova, V. & Moore, A. *In vivo* imaging of siRNA delivery and silencing in tumors. *Nature Med.* **13,** 372–377 (2007).
16. Naiden, E. *et al.* Magnetic properties and structural parameters of nanosized oxide ferrimagnet powders produced by mechanochemical synthesis from salt solutions. *Phys. Solid State* **5,** 891–900 (2003).
17. Bogdanov, A. A., Martin, C., Weissleder, R. & Brady, T. J. Trapping of dextran-coated colloids in liposomes by transient binding to aminophospholipid—preparation of ferrosomes. *Biochim. Biophys. Acta Biomembranes* **1193,** 212–218 (1994).
18. Di Paolo, D. *et al.* Liposome-mediated therapy of neuroblastoma. *Methods Enzymol.* **465,** 225–249 (2009).
19. Torchilin, V. P. *et al.* Poly(ethylene glycol) on the liposome surface - on the mechanism of polymer-coated liposome longevity. *Biochim. Biophys. Acta Biomembranes* **1195,** 11–20 (1994).
20. Fortin-Ripoche, J. P. *et al.* Magnetic targeting of magnetoliposomes to solid tumors with MR imaging monitoring in mice: feasibility. *Radiology* **239,** 415–424 (2005).
21. Martina, M. S. *et al.* Generation of superparamagnetic liposomes revealed as highly efficient MRI contrast agents for *in vivo* imaging. *J. Am. Chem. Soc.* **127,** 10676–10685 (2005).
22. Stollfuss, J. C. *et al.* Rectal carcinoma: high-spatial-resolution MR imaging and T2 quantification in rectal cancer specimens. *Radiology* **241,** 132–141 (2006).
23. Seo, W. S. *et al.* FeCo/graphitic-shell nanocrystals as advanced magnetic-resonance-imaging and near-infrared agents. *Nature Mater.* **5,** 971–976 (2006).
24. Ai, H. *et al.* Magnetite-loaded polymeric micelles as ultrasensitive magnetic-resonance probes. *Adv. Mater.* **17,** 1949–1952 (2005).
25. Shapiro, M. G., Atanasijevic, T., Faas, H., Westmeyer, G. G. & Jasanoff, A. Dynamic imaging with MRI contrast agents: quantitative considerations. *Magn. Reson. Imaging* **24,** 449–462 (2006).
26. Na, H. B. *et al.* Development of a T1 contrast agent for magnetic resonance imaging using MnO nanoparticles. *Angew Chem. Int. Ed.* **46,** 5397–5401 (2007).
27. Zhao, M., Josephson, L., Tang, Y. & Weissleder, R. Magnetic sensors for protease assays. *Angew Chem. Int. Ed.* **42,** 1375–1378 (2003).
28. Atanasijevic, T., Shusteff, M., Fam, P. & Jasanoff, A. Calcium-sensitive MRI contrast agents based on superparamagnetic iron oxide nanoparticles and calmodulin. *Proc. Natl Acad. Sci. USA* **103,** 14707–14712 (2006).
29. Guy, C. T., Cardiff, R. D. & Muller, W. J. Induction of mammary tumors by expression of polyomavirus middle T oncogene: a transgenic mouse model for metastatic disease. *Mol. Cell Biol.* **12,** 954–961 (1992).
30. Wender, P. A. *et al.* Real-time analysis of uptake and bioactivatable cleavage of luciferin-transporter conjugates in transgenic reporter mice. *Proc. Natl Acad. Sci. USA* **104,** 10340–10345 (2007).
31. Greenbaum, D., Medzihradszky, K. F., Burlingame, A. & Bogyo, M. Epoxide electrophiles as activity-dependent cysteine protease profiling and discovery tools. *Chem. Biol.* **7,** 569–581 (2000).
32. Greenbaum, D. *et al.* Chemical approaches for functionally probing the proteome. *Mol. Cell Proteomics* **1,** 60–68 (2002).
33. Joyce, J. A. *et al.* Cathepsin cysteine proteases are effectors of invasive growth and angiogenesis during multistage tumorigenesis. *Cancer Cell* **5,** 443–453 (2004).
34. Bell-McGuinn, K., Garfall, A., Bogyo, M., Hanahan, D. & Joyce, J. A. Inhibition of cysteine cathepsin protease activity enhances chemotherapy regimens by decreasing tumor growth and invasiveness in a mouse model of multistage cancer. *Cancer Res.* **67,** 7378–7385 (2007).
35. Schurigt, U. *et al.* Trial of the cysteine cathepsin inhibitor JPM-OEt on early and advanced mammary cancer stages in the MMTV-PyMT-transgenic mouse model. *Biol. Chem.* **389,** 1067–1074 (2008).
36. Vasiljeva, O. *et al.* Tumor cell-derived and macrophage-derived cathepsin B promotes progression and lung metastasis of mammary cancer. *Cancer Res.* **66,** 5242–5250 (2006).
37. Vasiljeva, O. & Turk, B. Dual contrasting roles of cysteine cathepsins in cancer progression: apoptosis versus tumour invasion. *Biochimie* **90,** 380–386 (2008).
38. Sevenich, L. *et al.* Synergistic antitumor effects of combined cathepsin B and cathepsin Z deficiencies on breast cancer progression and metastasis in mice. *Proc. Natl Acad. Sci. USA* **107,** 2497–2502 (2010).
39. Gocheva, V. & Joyce, J. A. Cysteine cathepsins and the cutting edge of cancer invasion. *Cell Cycle* **6,** 60–64 (2007).
40. Turk, V., Kos, J. & Turk, B. Cysteine cathepsins (proteases)—on the main stage of cancer? *Cancer Cell* **5,** 409–410 (2004).
41. Rossi, A., Deveraux, Q., Turk, B. & Sali, A. Comprehensive search for cysteine cathepsins in the human genome. *Biol. Chem.* **385,** 363–372 (2004).
42. Mohamed, M. M. & Sloane, B. F. Cysteine cathepsins: multifunctional enzymes in cancer. *Nature Rev. Cancer* **6,** 764–775 (2006).
43. Vasiljeva, O. *et al.* Emerging roles of cysteine cathepsins in disease and their potential as drug targets. *Curr. Pharm. Des.* **13,** 387–403 (2007).
44. Sloane, B. F. *et al.* Cathepsin B and tumor proteolysis: contribution of the tumor microenvironment. *Semin. Cancer Biol.* **15,** 149–157 (2005).
45. Gocheva, V. *et al.* IL-4 induces cathepsin protease activity in tumor-associated macrophages to promote cancer growth and invasion. *Genes Dev.* **24,** 241–255 (2010).
46. Ceelen, W. P. & Flessner, M. F. Intraperitoneal therapy for peritoneal tumors: biophysics and clinical evidence. *Nature Rev. Clin. Oncol.* **7,** 108–115 (2010).
47. Sadaghiani, A. M. *et al.* Design, synthesis, and evaluation of *in vivo* potency and selectivity of epoxysuccinyl-based inhibitors of papain-family cysteine proteases. *Chem. Biol.* **14,** 499–511 (2007).
48. Vasiljeva, O. *et al.* Reduced tumour cell proliferation and delayed development of high-grade mammary carcinomas in cathepsin B-deficient mice. *Oncogene* **27,** 4191–4199 (2008).

Acknowledgements

The authors thank Yu.F. Ivanov (Tomsk Scientific Center) for transmission electron microscopy, G. Kapun (National Institute of Chemistry) for scanning electron microscopy, M. Škarabot (Jozef Stefan Institute) for atomic force microscopy, J. Ščančar and M. Vahčič (Jozef Stefan Institute) for flame atomic absorption spectrometry, I.V. Sukhodolo, R.I. Pleshko, A.N. Dzuman, I.V. Milto and L.M. Ogorodova (Siberian State Medical University) for help in the acute toxicity study, and A. Sepe, M. Butinar, M. Trstenjak-Prebanda and A. Petelin (Jozef Stefan Institute), O.G. Terekhova (Tomsk Scientific Center), M. Tacke and N. Klemm (Institut für Molekulare Medizin und Zellforschung) for technical and methodological assistance, G. Salvesen (Sanford-Burnham Medical Research Institute) for valuable discussions, and R.H. Pain (Jozef Stefan Institute) for critical reading of the manuscript. JPM-565 was kindly provided by the Drug Synthesis and Chemistry Branch, Developmental Therapeutics Program, Division of Cancer Treatment and Diagnosis, National Cancer Institute. The research leading to these results was supported in part by the European Community's Seventh Framework Programme FP7/2007-2011 (grant agreement no. 201279, Microenvimet, O.V., T.R., C.P. and B.T.), the Slovenian Research Agency (research grant no. P1-0140, B.T.), the Russian Foundation for Basic Research (project no. 07-04-12170, E.P.N.), the United States Civilian Research and Development Foundation (project no. Y4-C16-05, A.A.M and V.I.I.) and the DFG SFB 850 (to T.R., C.P. and R.Z.).

Author contributions

G.M., U.M., I.P., S.G.P., B.T. and O.V. conceived and designed the experiments. G.M., U.M., L.B. and O.V. performed the experiments. G.M., U.M., S.G.P., B.T. and O.V. analysed the data. T.R., C.P. and R.Z. contributed transgenic mouse models and animal imaging. M.B. contributed JPM-565 inhibitor. A.A.M., V.I.I., E.P.N. and S.G.P. supplied the magnetic nanoparticles. S.G.P., V.T., B.T. and O.V. supervised the project. G.M., S.G.P., B.T. and O.V. wrote the manuscript. All authors discussed the results and commented on the manuscript.

Additional information

The authors declare no competing financial interests. Supplementary information accompanies this paper at www.nature.com/naturenanotechnology. Reprints and permission information is available online at http://www.nature.com/reprints. Correspondence and requests for materials should be addressed to B.T. and O.V.